Journal of the Korean Physical Society, Vol. 34, No. 1, January 1999, pp. 24∼28

Scaling Behavior of Electronegative rf Discharge Plasmas

Tae Hun CHUNG

Department of Physics, Dong-A University, Pusan 604-714

(Received 18 August 1998)

For radio-frequency discharges of electronegative gases, one-dimensional equilibrium equations for plasma variables are formulated and the scaling formulae of the plasma variables are derived in terms of the control parameters. The control parameters consist of three parameters: p (pressure), l_p (half-system length), and P (power) or n_e (electron density). The classifications of the operating regions are performed according to the prevailing particle-loss mechanism (recombination-loss-dominated or ion-flux-loss-dominated) and according to the main heating mechanism (ohmic-heating-dominated or stochastic-heating-dominated). The variations of the charged particle densities with pressure and absorbed power are estimated and compared with the results of a particle-in-cell simulation.

I. INTRODUCTION

Electronegative gases have found numerous applications in plasma processing, such as thin-film etching and deposition. The presence of negative ions complicates the discharge phenomena. The number of equations governing the equilibrium is large, and the analysis becomes difficult [1]. The features which make the electronegative discharge markedly different from the electropositive case are the presence of both negative ions with a particular (*e.g.* parabolic) spatial distribution and volume recombination loss. The particular spatial distribution of negative ions affects the ion flux loss to the wall.

There have been many approaches to describe a radio-frequency electronegative plasma. Fluid models have been developed by many researchers [2–4]. However, fluid models have some limitations in keeping track of the various interacting species and take considerable computational resources. Spatially averaged global models have also been developed for various regions of rf discharge plasmas [1,5–8], and analytic equilibrium models have been proposed and compared with the experimental results and other simulation results [9,10]. The scaling of plasma variables (charged particle densities, sheath width, electron temperature, and plasma potential) with the control parameters gives useful information for the design and analysis of plasma sources [11–13]. Scaling can be obtained from a global model, but since such models do not describe the spatial distribution of charged particle, they may not preserve the essential scalings of plasma parameters with control parameters over a wide parameter range.

The purpose of this study is to obtain the scaling laws explicitly throughout the entire range of operating regions based on a one-dimensional equilibrium model and a global model. Since the scaling itself depends on the operating region, a classification of regions in parameter space is needed. In deriving the scaling formulae, we determine the prevailing particle-loss mechanism (recombination loss or ion flux loss), and the main heating mechanism (ohmic heating or stochastic heating). The control parameters consist of three parameters: p (pressure), l_p (half-system length), and P (power) or n_e (electron density). The discharge should exhibit different scalings of the operating parameters in different regions.

II. SCALING RELATIONS

We consider a discharge with three charged plasma species (positive ions, negative ions, and electrons). From Ref. 10, assuming a parabolic distribution of negative ions in the electronegative region and a constant electron density n_{e0}, we have

$$\frac{n_+}{n_{e0}} = \frac{n_-}{n_{e0}} + 1 = \alpha_0 \left(1 - \frac{x^2}{l^2}\right) + 1, \tag{1}$$

where $\alpha_0 = n_{-0}/n_{e0}$ and l is the half-length of the electronegative core region (Fig. 1). Here, we assume that the sheath width is very small. When substituted into the equilibrium equations for positive-ion and negative-ion charge balance, Eq. (1) gives

$$K_{iz} n_0 l = K_{rec} n_{e0} \left(\frac{8}{15}\alpha_0^2 + \frac{2}{3}\alpha_0\right) l + \frac{2\overline{D_{a+}}\alpha_0}{l}, \tag{2}$$

$$K_{att} n_0 l_p = K_{rec} n_{e0} \left(\frac{8}{15}\alpha_0^2 + \frac{2}{3}\alpha_0\right) l, \tag{3}$$

where K_{iz}, K_{att}, and K_{rec} are the ionization, the attachment, and the recombination rates, respectively, and

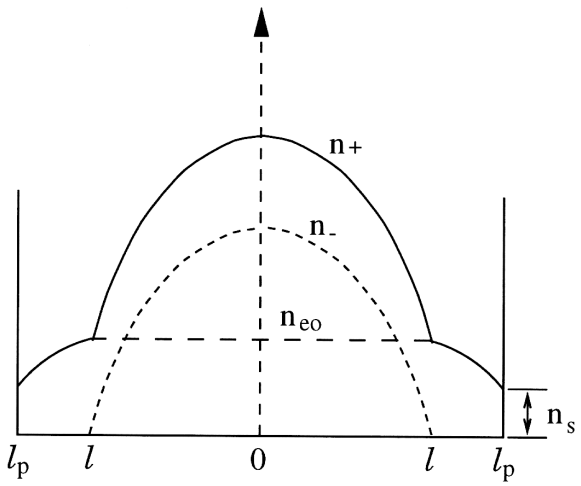

Typical one-dimensional profiles of the charged particle density. n_+, n_-, and n_e denote the positive-ion, the negative-ion and the electron density, respectively.

$\overline{D_{a+}}$ is obtained by averaging the ambipolar diffusion coefficient D_{a+} over a parabola and is given by

$$\overline{D_{a+}} \approx D_+ \frac{1+\gamma+2\gamma\bar{\alpha}}{1+\gamma\bar{\alpha}} \tag{4}$$

with $\bar{\alpha} = \frac{2}{3}\alpha_0$, and $\gamma = T_e/T_i$.

In the electropositive edge region, the positive-ion particle balance is

$$\frac{2\overline{D_{a+}}\alpha_0}{l} + K_{iz} n_0 (l_p - l) = h_l u_{B0}, \tag{5}$$

where $u_{B0} = (eT_e/M)^{1/2}$ and $h_l = n_s/n_{e0}$. At low pressures

$$h_l = \left[\frac{a + (u(l)/u_{B0})^3}{1+a}\right]^{1/3}, \tag{6}$$

where n_s is the electron (and positive ion) density at the plasma edge, $u(l)$ is the ion velocity leaving the electronegative core region ($= \frac{2\overline{D_{a+}}\alpha_0}{l}$), and $a = 2\nu_{iz}\lambda/\pi u_{B0}$ with $\nu_{iz} = K_{iz} n_0$ and λ being the ion mean free path [10].

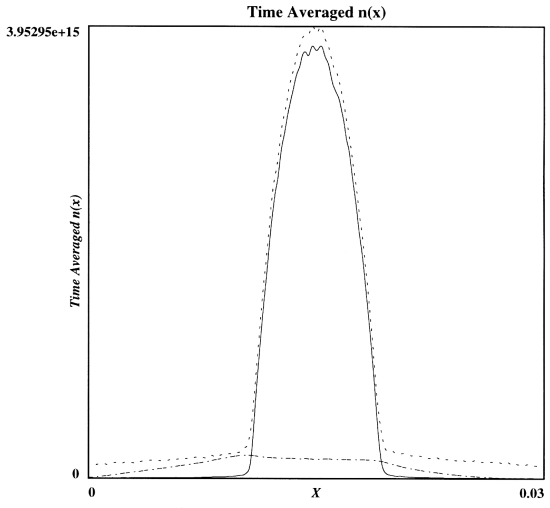

Fig. 2. One-dimensional charged particle density profiles obtained by a particle-in-cell simulation. The dotted, the solid, and the slashed lines represent the positive ions, the negative ions, and the electrons, respectively. Here $p = 0.1$ Torr, $V_{rf} = 200$ V, and $f = 10$ MHz.

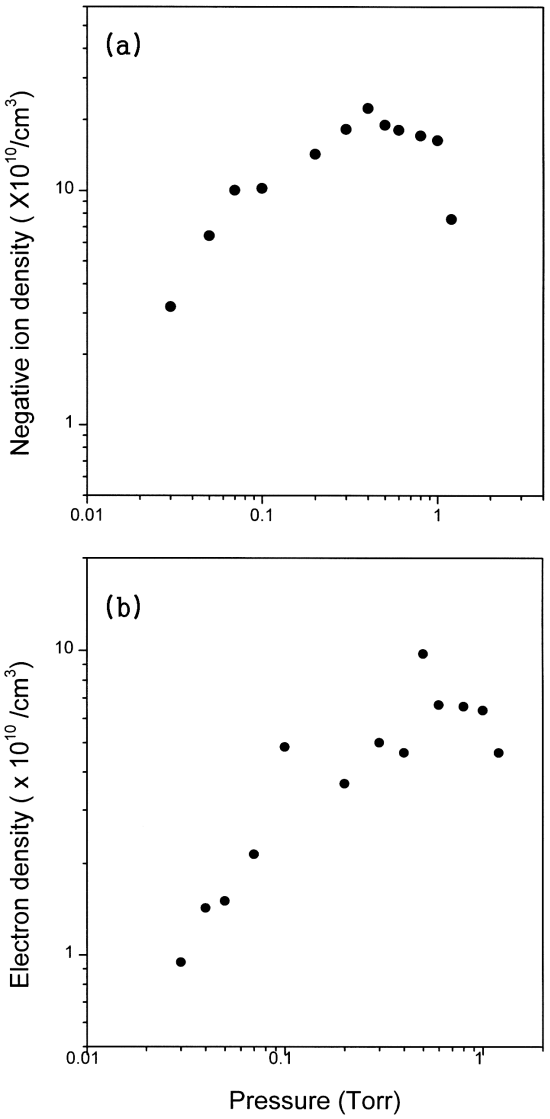

Fig. 3. (a) Average electron density vs pressure. (b) Average negative-ion density vs pressure. Here, $V_{rf} = 200$ V and $f = 10$ MHz.

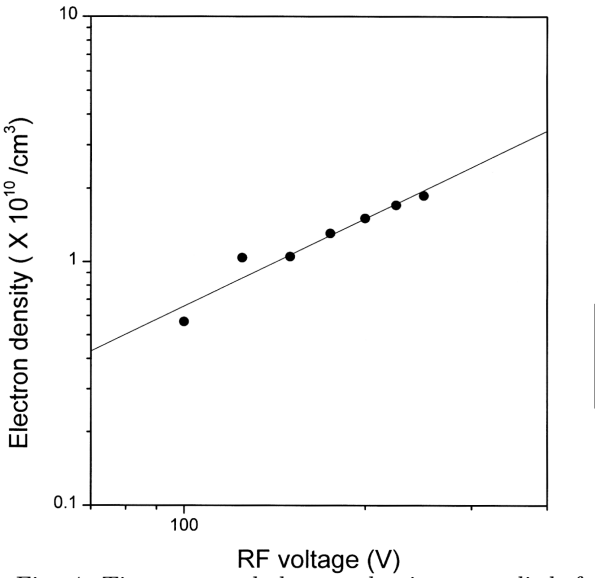

Fig. 4. Time-averaged electron density vs applied rf voltage.

Equations (2), (3), and (5) with Eqs. (1), (4), and (6) constitute a one-dimensional equilibrium model in which the three unknowns α_0, l, and T_e can be found from the input parameters n_{e0}, T_i, n_0, and l_p. A key parameter which separates the region treated above from the region in which the density distribution is flattened and volume effects are important is the ratio of the recombination flux to the flux leaving the system. Recognizing that the recombination flux and the attachment flux just balance, by Eq. (3), we can write these fluxes as $\Gamma_{rec} = K_{att} n_0 n_{e0} l_p$ and $\Gamma_+(l_p) = h_l n_{e0} u_{B0}$. The ratio that separates the surface-ion-flux- and the volume (recombination)-loss-dominated regions is

$$R_L = \frac{\Gamma_{rec}}{\Gamma_+(l_p)} = \frac{K_{att} n_0 l_p}{h_l u_{B0}}. \tag{7}$$

An intermediate transition exists for

$$(u(l)/u_{B0})^3 = a \tag{8}$$

and physically describes the transition in which the ion flux leaving the electronegative region is equal to the ion flux produced outside that region. Thus, for relatively small α_0 with l/l_p significantly less than 1, we use the approximation $a \gg (u(l)/u_{B0})^3$. We call this region the strong ion-flux-loss(IFL)-dominated region. Then, h_l can be approximated by

$$h_l \simeq a^{1/3} \simeq (\lambda/l_p)^{1/2} \simeq \frac{1}{(\sigma n_0 l_p)^{1/2}}. \tag{9}$$

The second approximate equality is obtained from a self-consistent analysis in the low-α_0 region (see the Appendix). We note that from Eq. (7)

$$R_L \approx \frac{K_{att}\sigma^{1/2}(n_0 l_p)^{3/2}}{u_{B0}} \propto (p l_p)^{3/2}. \tag{10}$$

The approximation of Eq. (9) is not, as we shall see below, valid near and above the transition of Eq. (8), where the opposite approximation holds:

$$h_l \simeq u(l)/u_{B0}. \tag{11}$$

Substituting Eq. (11) to Eq. (7), we can obtain

$$R_L = \frac{K_{att}\sigma N_0^2}{4 v_{th}\alpha_0} \propto \frac{(p l_p)^2}{(p/n_{e0})^{1/2}}. \tag{12}$$

In this weak IFL-dominated region, a detailed analysis gives the simple results $l/l_p \simeq 1$ and $\alpha_0 \simeq \left(\frac{15 K_{att} n_0}{8 K_{rec} n_{e0}}\right)^{1/2}$. In fact, it was shown [14] that there is a smooth transition to an approximate solution of a charged particle density with a flattened central region. Nevertheless, at the transition of Eq. (8), $l/l_p \simeq 1$ such that most of the ion flux is generated in the electronegative region; and therefore, the approximation of Eq. (11) is valid. In the recombination-loss-dominated region, where $\Gamma_{rec} \gg \Gamma_+(l_p)$, we have $l/l_p \simeq 1$,

$$R_L = \frac{\Gamma_{rec}}{\Gamma_+(l_p)} \approx \frac{\frac{8}{15} K_{rec} n_{e0} \alpha_0^2 l}{\frac{2\overline{D_{a+}}\alpha_0}{l}}, \tag{13}$$

and

$$\alpha_0 \simeq \bar{\alpha} \simeq \left(\frac{K_{att} n_0 l_p}{K_{rec} n_{e0} l_p}\right)^{1/2} \propto p^{1/2} n_{e0}^{-1/2}. \tag{14}$$

Thus, we obtain the scaling formula for R_L as

$$R_L \propto \frac{(p l_p)^2}{(p/n_{e0})^{1/2}}. \tag{15}$$

We note that the ratio R_L has the same functional form for both the weak IFL region and the recombination-loss-dominated regime. Thus, in higher power and higher pressure discharges the recombination loss mechanism becomes more dominant.

Although the electron density is a convenient scaling parameter, the absorbed power is the usual control parameter. If we use the total absorbed power as a control parameter, we must determine the power absorbed by the ions, as well as by the electrons. This requires a knowledge of the heating mechanisms. Here, we shall consider only the power absorbed by the electrons, P_{abse}, which may or may not approximate the total power P_{abs}.

For the parameter space where $\Gamma_{rec} \ll \Gamma_+(l_p)$, the electron absorbed power per unit area is, approximately [15],

$$P_{abse} \simeq n_{e0} h_l u_{B0} (\varepsilon_c + 2T_e), \tag{16}$$

where ε_c is the energy lost per ionization, which is much more for a diatomic gas than for a monatomic gas, especially at low temperature, and is dominated by the excitation loss [1]

$$\varepsilon_c \simeq \varepsilon_{iz} + \frac{K_{exc}}{K_{iz}}\varepsilon_{exc} \simeq \frac{K_{exc}}{K_{iz}}\varepsilon_{exc}. \tag{17}$$

Using the approximate flux condition in which the recombination loss is very small, we have

$$K_{iz} n_{e0} n_0 l_p \simeq n_{e0} h_l u_{B0}; \tag{18}$$

then, substituting for ε_c in Eq. (16), with $T_e \ll \varepsilon_c$, we have $P_{abse} \simeq n_{e0} n_0 l_p K_{exc} \varepsilon_{exc}$ which gives the scaling

$$n_{e0} \propto \frac{P_{abse}}{p l_p}. \tag{19}$$

In the recombination-loss-dominated region, where $\Gamma_{rec} \gg \Gamma_+(l_p)$, the power absorbed per unit area is [5,15]

$$P_{abse} \simeq K_{rec} n_+ n_- l_p \varepsilon_c. \tag{20}$$

Noting $n_+ \simeq n_-$ with $\varepsilon_c \simeq K_{exc}\varepsilon_{exc}/K_{iz}$ and $K_{iz} \simeq K_{att}$, we have

$$n_+ \propto \frac{P_{abse}^{\frac{1}{2}}}{l_p^{\frac{1}{2}}}, \tag{21}$$

and with α_0 from Eq. (14),

$$n_{e0} \propto \frac{P_{abse}}{p l_p}. \tag{22}$$

Thus, n_{e0} scales the same with P_{abse} and p in both regions. In the intermediate region, we have

$$n_{e0} \propto \frac{P_{abse}}{(p l_p)^y}, (0 < y < 1). \tag{23}$$

The argument y depends on the ratio of the recombination loss to the total loss.

Some modifications are needed when we consider plasma heating. To illustrate this, we will consider the example of a symmetric rf capacitive discharge of high aspect ratio. In capacitive discharges, it is generally necessary to consider the power lost to the ions as well as the power lost to the electrons. For an rf voltage V_1 across each sheath, there is a d.c component, to prevent electron loss, of approximately $\bar{V} \simeq 0.8 V_1$, which accelerates the ions [15]. For $\Gamma_{rec} \ll \Gamma_+(l_p)$ the total absorbed power is

$$P_{abs} = n_{e0} h_l u_{B0} (\varepsilon_c + 2T_e + \bar{V}). \tag{24}$$

If $V_1 \gg \varepsilon_c$, then we have the ratio

$$\frac{P_{abs}}{P_{abse}} \simeq \frac{V_1}{\varepsilon_c} \tag{25}$$

such that P_{abs} (stochastic heating) $\propto V_1^2$ and P_{abs} (ohmic heating) $\propto V_1^{3/2}$ [16]. In this region and with $h_l \approx (\lambda/l_p)^{1/2}$, we have

$$n_{e0} \approx \frac{P_{abs}(l_p/\lambda)^{\frac{1}{2}}}{0.8 V_1 u_{B0}}. \tag{26}$$

For stochastic heating with $P_{abs} \propto V_1^2$,

$$n_{e0} \propto P_{abs}^{\frac{1}{2}} (p l_p)^{\frac{1}{2}} \tag{27}$$

while for ohmic heating with $P_{abs} \propto p l_p V_1^{\frac{3}{2}}$,

$$n_{e0} \propto P_{abs}^{\frac{1}{3}} (p l_p)^{\frac{7}{6}}. \tag{28}$$

For the weak IFL region, the negative ion density scales as

$$n_- = n_{e0}\alpha_0 \simeq n_{e0}^{\frac{1}{2}} p^{\frac{1}{2}}. \tag{29}$$

In the opposite limit, for $\Gamma_{rec} \gg \Gamma_+(l_p)$, we generally have

$$\Gamma_{rec}\varepsilon_c \gg \Gamma_+(l_p) V_1 \tag{30}$$

such that no change in the scaling in Eqs. (21) - (23) is required. Clearly, there are intermediate ranges of parameters for which no simple scaling exists. The electron temperature dependence on pressure for low pressure electronegative discharges is similar to that for electropositive discharges [1]. As the pressure increases, the electron temperature decreases, and the collisional energy loss ε_c increases drastically, which makes ε_c greater than V_1. Thus, at medium or high pressures, P_{abse} becomes comparable to P_{abs}. Therefore, Eqs. (25) and (26) are not valid in the medium- or high-pressure region, even for capacitively coupled discharges. For low sheath voltages which occur in inductively coupled discharges, $\bar{V}$ is small compared to ε_c; thus, we can assume $P_{abs} \simeq P_{abse}$. From this argument, we can infer that for inductively coupled discharges, the scaling formulae of Eqs. (19), (21), and (22) can be used without considering the detailed heating mechanisms.

III. COMPARISON WITH SIMULATION RESULTS

In this study, we use a particle-in-cell (PIC) simulation to verify the obtained scaling formula. Capacitively coupled electronegative oxygen plasmas are studied in one dimension by using a bounded PIC simulation code with Monte Carlo collisions (XPDP1) [17]. For purposes of comparison, the simulated device is assumed to have 0.01 m^2 electrodes separated by 3 cm and to be operated at 10 MHz. The blocking capacitance in the external circuit is chosen to be $C_b = 628$ nF. The applied rf voltage is held at 200 V, and the neutral gas pressure is varied from 30 mTorr to 1.2 Torr. The secondary electron emission coefficient due to ion bombardment to the electrode is arbitrarily chosen to be 0.2. Figure 2 shows the charged particle density profiles obtained from the PIC simulation.

The pressure dependencies of the electron density and the negative-ion density are shown in Fig. 3. At low pressure, the negative-ion density increases with pressure, but at medium or high pressure, it decreases again after a little saturation. This indicates a transition of scaling from Eq. (29) to Eq. (19). We obtained similar scalings

for a chlorine discharge by using a two-dimensional fluid simulation [4]. Although not shown in the figures, we observed that as the pressure increased, the density profiles of the positive and the negative ions changed from a parabolic to a flat-top configuration. In a sophisticated model [18] in which various reactions involving neutral atoms are considered, the situation becomes more complicated. However, in this simple reaction model in which the reactions of neutral atoms are neglected, the balance of negative ions is governed by dissociative attachment and ion-ion recombination, which causes the negative-ion density to increase as the square root of pressure at low pressures and to decrease at high pressures. Also, it should be noted that the formulation in this simulation assumes a low degree of dissociation and an abundance of molecular ions (for example, $O_2^+ \gg O^+$), which is attributed to the ready recombination of neutral atoms on the chamber walls.

In Fig. 4, we show the electron density as a function of the applied rf voltage. The electron density scales as $V_{rf}^{1.19}$, which can be compared with Eqs. (27) and (28).

IV. CONCLUSION

Based on a global model and a one-dimensional equilibrium model, we have proposed a scaling formulae for electronegative plasmas with three charged species. The estimated scalings are compared well with the results of PIC simulations. The extension to four charged species is under consideration, and an experimental study is being performed to verify these scalings more carefully.

ACKNOWLEDGMENTS

The author is very grateful to Professors A. J. Lichtenberg and M. A. Lieberman of the University of California at Berkeley for their helpful suggestions. This work is supported by Dong-A University and by the Basic Science Research Institute Program, Korea Ministry of Education (BSRI-97-2439).

V. APPENDIX

If we neglect recombination, the number of positive ions generated is approximately equal to the number lost to the wall:

$$\nu_{iz} n_{e0} l_p \simeq u_{B0} h_l n_{e0}. \tag{31}$$

If we apply $h_l \simeq a^{1/3}$, then

$$\nu_{iz} l_p \simeq u_{B0} \left(\frac{2\nu_{iz}\lambda}{\pi u_{B0}} \right)^{1/3}, \tag{32}$$

$$\nu_{iz}^{2/3} \simeq \frac{u_{B0}^{2/3}}{l_p^{2/3}} \left(\frac{2\lambda}{\pi l_p} \right)^{1/3}, \tag{33}$$

$$h_l \simeq \left(\frac{2\lambda}{\pi u_{B0} l_p} \right)^{1/3} \left(\frac{2\lambda}{\pi l_p} \right)^{1/6} u_{B0}^{1/3}. \tag{34}$$

Finally, we have

$$h_l \simeq \left(\frac{2\lambda}{\pi l_p} \right)^{1/2}. \tag{35}$$

REFERENCES

[1] C. Lee and M. A. Lieberman, J. Vac. Sci. Technol. **A13**, 368 (1995).
[2] S. K. Park and D. J. Economou, J. Appl. Phys. **68**, 3904 (1990).
[3] T. J. Sommerer and M. J. Kushner, J. Vac. Sci. Technol. **B10**, 2179 (1992).
[4] T. H. Chung, L. Meng, H. J. Yoon and J. K. Lee, Jpn. J. Appl. Phys. **36**, 2874 (1997).
[5] Y. T. Lee, M. A. Lieberman, A. J. Lichtenberg, F. Bose, H. Baltes and R. Patrick, J. Vac. Sci. Technol. **A15**, 113 (1997).
[6] M. A. Lieberman and S. Ashida, Plasma Sources Sci. Technol. **5**, 145 (1996).
[7] N. S. Yoon, S. S. Kim, C. S. Chang and D. I. Choi, J. Korean Phys. Soc. **28**, 172 (1995).
[8] M. Yoon, S. C. Kim, H. J. Lee and J. K. Lee, J. Korean Phys. Soc. **32**, 635 (1998).
[9] A. J. Lichtenberg, V. Vahedi, M. A. Lieberman and T. Rognlien, J. Appl. Phys. **75**, 2339 (1994).
[10] I. G. Kouznetsov, A. J. Lichtenberg and M. A. Lieberman, Plasma Sources Sci. Technol. **5**, 662 (1996).
[11] G. A. Hebner, J. Appl. Phys. **81**, 578 (1997).
[12] T. Mieno, T. Kamo, D. Hayashi, T. Shoji and K. Kadota, Appl. Phys. Lett. **69**, 617 (1996).
[13] J. H. Park and S. H. Hong, J. Korean Phys. Soc. **31**, 753 (1997).
[14] A. J. Lichtenberg, I. G. Kouznetsov, Y. T. Lee, M. A. Lieberman, I. D. Kaganovich and L. D. Tsendin, Plasma Sources Sci. Technol. **6**, 437 (1997).
[15] M. A. Lieberman and A. J. Lichtenberg, *Principles of Plasma Discharges and Materials Processing* (Wiley, New York, 1994).
[16] T. H. Chung, H. S. Yoon and J. K. Lee, J. Appl. Phys. **78**, 6441 (1995).
[17] C. K. Birdsall, IEEE Trans. Plasma Sci. **19**, 65 (1991).
[18] E. Stoffels, W. W. Stoffels, D. Vender, M. Kando, G. M. W. Kroesen and F. J. de Hoog, Phys. Rev. **E51**, 2425 (1995).